





## Open Archive Toulouse Archive Ouverte (OATAO)

OATAO is an open access repository that collects the work of Toulouse researchers and makes it freely available over the web where possible

This is an author's version published in: <http://oatao.univ-toulouse.fr/21619>

**Official URL:** <https://doi.org/10.1021/acs.cgd.6b00834>

### To cite this version:

Torré, Jean-Philippe  and Coupan, Romuald and Chabod, Mathieu and Péré, Eve and Labat, Stéphane and Khoukh, Abdel and Brown, Ross and Sotiropoulos, Jean-Marc and Gornitzka, Heinz  *CO<sub>2</sub>-Hydroquinone Clathrate: Synthesis, Purification, Characterization and Crystal Structure*. (2016) *Crystal Growth & Design*, 16 (9). 5330-5338. ISSN 1528-7483

Any correspondence concerning this service should be sent to the repository administrator: [tech-oatao@listes-diff.inp-toulouse.fr](mailto:tech-oatao@listes-diff.inp-toulouse.fr)

# CO<sub>2</sub>–Hydroquinone Clathrate: Synthesis, Purification, Characterization and Crystal Structure

Jean-Philippe Torr ,\*,† Romuald Coupan,† Mathieu Chabod,† Eve Pere,‡ St phane Labat,‡ Abdel Khoukh,‡ Ross Brown,‡ Jean-Marc Sotiropoulos,‡ and Heinz Gornitzka<sup>§,||</sup>

†Universit  Pau & Pays Adour, Laboratoire des Fluides Complexes et leurs R servoirs (LFCR), UMR CNRS 5150, Avenue de l'Universit , BP 1155, F-64013, Pau, France

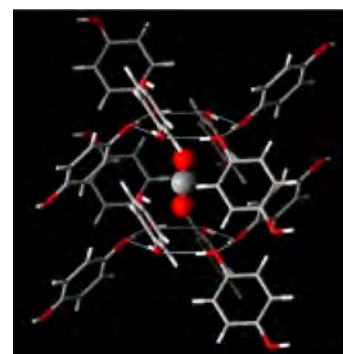
‡Universit  Pau & Pays Adour, Institut des Sciences Analytiques et de Physico-Chimie pour l'Environnement et les Mat riaux (IPREM), UMR CNRS 5254, H lioparc, Av. du Pr sident Pierre Angot, F-64000 Pau, France

§CNRS, LCC (Laboratoire de Chimie de Coordination), 205 route de Narbonne, BP 44099, F-31077 Toulouse Cedex 4, France

||Universit  de Toulouse, UPS, INPT, F-31077 Toulouse Cedex 4, France

## Supporting Information

**ABSTRACT:** Organic clathrate compounds, particularly those formed between hydroquinone (HQ) and gases, are supramolecular entities recently highlighted as promising alternatives for applications such as gas storage and separation processes. This study provides new insights into CO<sub>2</sub>–HQ clathrate, which is a key structure in some of the proposed future applications of these compounds. We present a novel synthesis and purification of CO<sub>2</sub>–HQ clathrate monocrystals. Clathrate crystals obtained from a single synthesis and native HQ are characterized and compared using Raman/Fourier transform infrared/NMR spectroscopies, optical microscopy, and thermogravimetric analysis coupled to mass spectrometry. The molecular structure of the clathrate has been resolved by X-ray diffraction analysis, and detailed crystallographic information is presented for the first time.



## INTRODUCTION

Clathrates are supramolecular compounds formed by inclusion of molecules of a guest in cavities of a crystalline framework of a host species, without forming any specific bond between guest and host.<sup>1</sup> Hydroquinone (HQ), a phenolic compound of formula *p*-C<sub>6</sub>H<sub>4</sub>(OH)<sub>2</sub> called quinol in the older literature, is well-known to form organic clathrates by encapsulating guest molecules of various sizes such as methanol, hydrogen sulfide, methane, carbon dioxide, or acetonitrile.<sup>2</sup> There are three common polymorphs of HQ, the  $\alpha$ ,  $\beta$ , and  $\gamma$  forms, the most versatile being the  $\beta$  form, which is the clathrate structure. Interestingly, another phase of hydroquinone ( $\delta$ -HQ) was detected recently at high pressure and temperature.<sup>3</sup>

The  $\beta$  form of HQ was first described by Powell and co-workers in the 1940s.<sup>4,5</sup> Figure 1 shows, as an example, a clathrate structure formed by HQ and xenon.<sup>6</sup>

HQ molecules, in the presence of suitable guest species and in specific experimental conditions, are able to combine to form a solid inclusion compound (i.e., the clathrate), where the guest molecule is encapsulated in the cavities formed by the host framework. Such clathrates, see Figure 1, can be described as two mutually interpenetrating, unconnected networks of HQ molecules, forming a cavity between two nearly planar hexagonal rings composed of hydrogen bonds between adjacent HQ molecules. The general formula is  $xG\cdot 3C_6H_4(OH)_2$ , where  $x$  is the site-occupancy factor of the guest (between zero and

one), and G is the encapsulated guest molecule. The ideal stoichiometry is one guest molecule per 3 HQ. However, these compounds are very often nonstoichiometric and stable with incomplete filling of all the cavities. The HQ clathrates have a rhombohedral unit cell. However, the space group depends on the guest species, and three crystallographic types of clathrates of same general formula can be defined (types I, II, and III).<sup>7</sup> The structure of type I HQ clathrates is centrosymmetric with space group  $R\bar{3}$ . It is known to be formed with small guests such as for example Xe or H<sub>2</sub>S. Type II clathrates are formed by larger guests such as methanol or HCl, with loss of centrosymmetry and space group  $R3$ .<sup>8</sup> Type III exhibits a further lowering of the symmetry to space group  $P3$ , with three distinct types of trigonal cavities which have the shape of prolate spheroids.<sup>2</sup> This form is obtained with CH<sub>3</sub>CN, which takes three individual and well-defined orientations inside the cavities.<sup>9</sup>

The  $\alpha$ -polymorph is the stable form of HQ under ambient conditions, space group  $R\bar{3}$ , with 54 HQ molecules in the primitive hexagonal unit cell, grouped in 18 asymmetric unit of three HQ molecules.<sup>10</sup> Interestingly, only two of these three molecules are involved in interpenetrating hydrogen-bonded

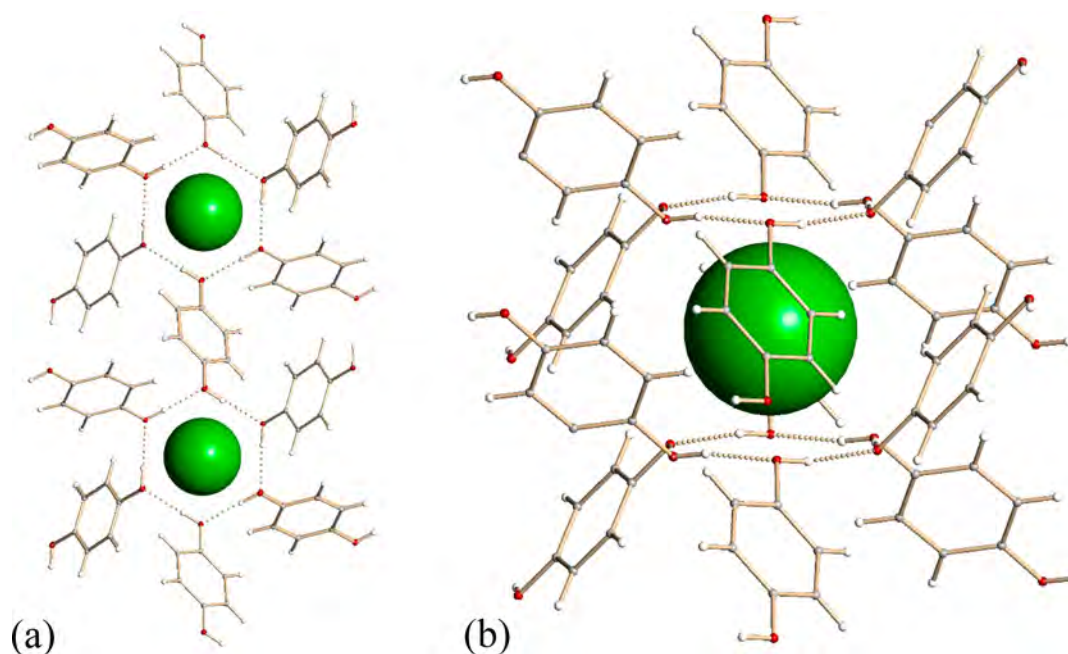


**Figure 1.** Schematic view of a HQ clathrate of xenon. (a) Top view with the  $c$  axis perpendicular to the figure; (b) the cavity shown in perspective. The xenon atom is represented by the green sphere.

networks similar to those found in the  $\beta$ -form, forming cavities able to accommodate small guest molecules such as  $\text{SO}_2$ ,<sup>11</sup> Ar,<sup>12</sup>  $\text{H}_2$ ,<sup>13</sup> and  $\text{CO}_2$ .<sup>4</sup> The third molecule participates in double helix chains of hydrogen-bonded HQ molecules. Hydrogen bonds connect HQ molecules in the interpenetrating networks to those in the helices. These connections drastically reduce the number of cavities compared to the  $\beta$ -form, giving a maximum occupancy of 1 guest for 18 host molecules for this structure.

The HQ  $\gamma$ -form can be obtained by slow evaporation of the solvent from an ether solution containing HQ. The structure is monoclinic, space group  $P2_1/c$ , formed by sheets of hydrogen bonded HQ molecules, held together by van der Waals forces.<sup>14</sup> No hydrogen bonded hexameric unit is present in this structure, and the  $\gamma$ -form is not known to have inclusion properties.<sup>2</sup>

Finally, the  $\delta$  form of HQ, reported by Naoki and co-workers in 1999, exists only at high pressure and temperature (for example, the  $\alpha$  to  $\delta$  transition temperature and the melting temperature of the  $\delta$  phase were estimated at  $\sim 170.2$  °C and  $\sim 191.4$  °C, respectively, at 785 bar).<sup>3</sup> Although this new  $\delta$  phase exhibits interesting properties, for example, a heat capacity much higher than that of  $\alpha$  phase (close to that of the liquid), its structure is unknown to date.<sup>15</sup>

Besides being fascinating scientific curiosities for more than a century, HQ clathrates deserve increasing attention in possible practical applications such as sequestration of dangerous substances such as radioactive kryptonate,<sup>16</sup> hydrogen storage,<sup>17,18</sup> and gas separation processes by selective clathration.<sup>19,20</sup>

Since the 1990s, much effort has been devoted to finding effective strategies and novel materials for large-scale reduction of carbon dioxide emission, by capture, sequestration, and  $\text{CO}_2$  recycling.<sup>21,22</sup> HQ clathrates have been proposed as promising materials for efficient  $\text{CO}_2$  separation because the HQ clathrate formed in the presence of a gas mixture containing  $\text{CO}_2$  (e.g.,  $\text{CO}_2/\text{H}_2$ ,  $\text{CO}_2/\text{CH}_4$ ,  $\text{CO}_2/\text{N}_2$ ) may be very selective to this gas.<sup>23–25</sup> Theoretical aspects were recently revisited to properly

model phase equilibria of type I gas organic clathrates formed with HQ,<sup>26</sup> but unfortunately the thermodynamical modeling was not extended to  $\text{CO}_2$ -HQ clathrate, principally for two reasons: (i) the complex, presumably nonspherical structure of the cage encapsulating  $\text{CO}_2$ ; (ii) the absence of a detailed (atomistic) experimental structure, preventing accurate calculation of some model parameters. Molecular dynamics or quantum calculations are difficult for the same reasons. Fortunately, although no real structure analysis of  $\text{CO}_2$ -HQ clathrate has been published to date, data on its phase equilibrium have been published very recently,<sup>27</sup> providing the thermodynamic information necessary to synthesize monocrystals. Thus, providing structural, physical, and chemical characterization data of the  $\text{CO}_2$ -HQ clathrate appears of great importance for fundamental purposes, novel clathrate-based experimental developments, and future applications.

HQ clathrates are generally obtained by recrystallization from solution, where the host molecules (HQ), the guest species (here  $\text{CO}_2$ ), and a solvent which cannot be clathrated, are brought together and cooled together.<sup>28</sup> One of the limitations of such a protocol is the variation of temperature during the synthesis, which could render some data (such as the clathrate occupancy) difficult to analyze as the synthesis conditions are not isothermal.<sup>29</sup> Here, we describe a novel synthesis and purification protocol for obtaining  $\text{CO}_2$ -HQ clathrate monocrystals. These crystals are characterized by various complementary techniques—Raman/infrared and  $^{13}\text{C}$  NMR spectroscopies, microscopy imaging, thermogravimetric analysis coupled to mass spectroscopy (ATG/SM)—and the results obtained are presented and discussed. Finally, the arrangement of the host and guest molecules in the solid state is determined by X-ray diffraction.

## ■ EXPERIMENTAL SECTION

**Synthesis and Purification of  $\text{CO}_2$ -HQ Crystals.** The experimental apparatus and materials are described in the [Supporting Information](#) (SI). The quantities of HQ and ethanol were adjusted

such that the solution at 298 K was oversaturated in HQ, according to the solubility data and correlation proposed by Li et al.<sup>30</sup> Typically, the quantities of HQ and ethanol used for the synthesis were 8 and 11 g, respectively. The two products were weighed into a glass vessel which was carefully introduced in the high pressure reactor. The whole system was then closed, the temperature was regulated at  $298.0 \pm 0.1$  K, and the magnetic stirrer started to properly dissolve HQ in the solvent. Stirring was stopped after a period of about 30 min, and the solution was left in static conditions until the end of the synthesis. The reactor was then evacuated to remove the air initially present and slowly pressurized with CO<sub>2</sub> at 0.1 bar per min until reaching a pressure of 20 bar. Crystallization was monitored continuously with the camera during the subsequent 20 h reaction time.

At the beginning of the synthesis (see Figure 2a), the system is a clear (over)saturated solution of HQ dissolved in ethanol with remaining  $\alpha$ -HQ crystallites settled to the bottom of the glass vessel. During pressurization, a solid crust forms first at the gas/liquid interface (see Figure 2b), and small crystallites (needles) begin to grow downward from this interface. The thickness of the crust increases during pressurization, while needles are also formed at the bottom of the vessel, as clearly shown in Figure 2c. After 20 h of reaction, the crystallization is complete, and the bulk is full of crystals as seen in Figure 2d. At the end of the synthesis, the reactor is depressurized from 20 to 1 bar at 0.5 bar per minute and opened rapidly to perform the CO<sub>2</sub>-HQ clathrate crystal purification. The glass vessel, which contains a suspension of crystals in ethanol, is carefully extracted from the reactor.

The crystals were washed before filtration to avoid  $\alpha$ -HQ crystallizing at their surface by evaporation of the thin film of solution (HQ-saturated ethanol) which coats the crystals. Therefore, the suspension obtained from the synthesis (i.e., a mixture of ethanol and crystals) was poured immediately after extraction into a sufficient volume of CH<sub>2</sub>Cl<sub>2</sub>. The crystals, which are not soluble in CH<sub>2</sub>Cl<sub>2</sub>, were perfectly washed with this solvent, and ethanol (immiscible and less dense than CH<sub>2</sub>Cl<sub>2</sub>) could be easily eliminated. Once the crystals were washed, the temperature of the suspension, now HQ crystals in CH<sub>2</sub>Cl<sub>2</sub>, was adjusted so that the density of CH<sub>2</sub>Cl<sub>2</sub> allowed efficient separation of the two populations of  $\alpha$ -HQ and clathrate crystals. A temperature in the range of 5–7 °C was found to be appropriate.  $\alpha$ -HQ crystals, which are less dense than the clathrate ones, can be eliminated at the top of the Büchner funnel, and only the heavier crystals (settled on the Büchner filter) were conserved for the next step. The vacuum system of the Büchner was then turned on to eliminate the CH<sub>2</sub>Cl<sub>2</sub> by filtration. Finally, the CO<sub>2</sub>-HQ clathrate crystals were dried under ambient conditions for further characterization and analysis. Contrary to crystals observed inside the reactor at the end of the synthesis, that appear perfectly transparent (see Figure 2d), the dried crystals appear opaque to the naked eye.

## RESULTS AND DISCUSSION

**Chemical and Physical Characterization of the Crystals.** The crystals were analyzed (within a few minutes to 2 h maximum after the end of the purification step) by using several analytical and complementary techniques: Raman, FT-IR, and <sup>13</sup>C NMR spectroscopies, optical microscopy, and thermogravimetric analysis coupled to mass spectroscopy (TGA/MS). The characterization methods are described in SI. The value of Raman, FT-IR, and NMR spectroscopies is well-known to distinguish between the native form ( $\alpha$ -HQ) and the CO<sub>2</sub>-HQ clathrate, while providing important information on the purity of the analyzed crystals.<sup>31–33</sup> Optical microscopy was used to obtain data on the morphology of the crystals. TGA/MS was used to analyze the thermal response of the crystals and to obtain the quantity of gas encapsulated in the clathrate (i.e., the clathrate occupancy) in the synthesis conditions. It is worth noting that it is the first time that such a collection of characterizations has been realized on the

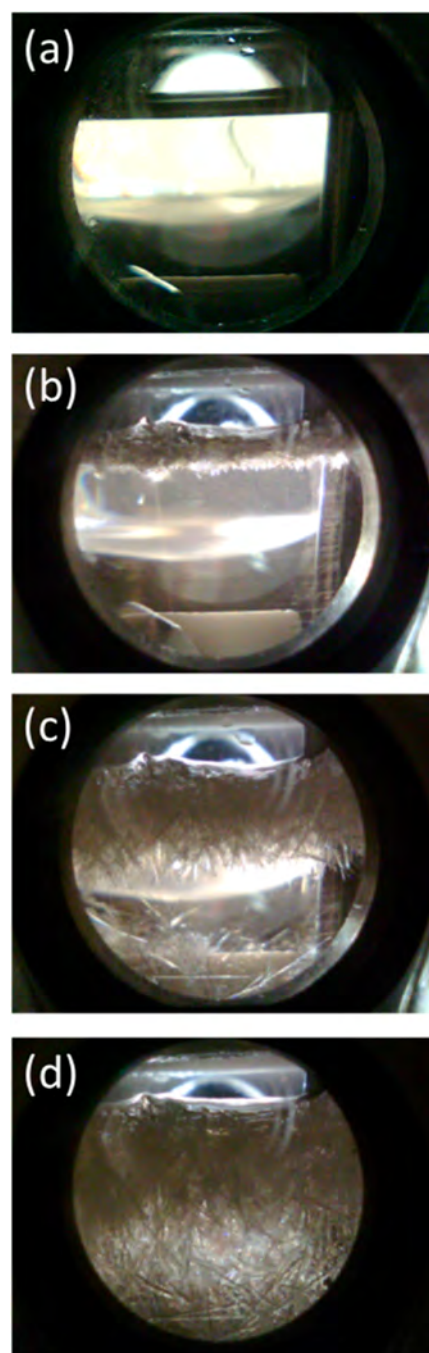


**Figure 2.** Snapshots taken through the reactor window during the crystal synthesis: (a)  $t = 15$  min; (b)  $t = 30$  min; (c)  $t = 117$  min; (d)  $t = 1200$  min. The initial time ( $t = 0$ ) corresponds to the start of reactor pressurization.

same CO<sub>2</sub>-HQ clathrate sample and compared to the native crystals ( $\alpha$ -HQ). The technical specifications of the instruments and the methods used to perform these characterizations are detailed in the SI.

**Raman, Infrared, and <sup>13</sup>C NMR Spectroscopic Analysis.** First, Figure 3 shows the Raman spectra of the native  $\alpha$ -HQ and our CO<sub>2</sub>-HQ clathrate sample.

It is logical to observe some similarity between the two spectra, as the same covalent bonds exist in both phases (i.e.,  $\alpha$ - and  $\beta$ -HQ).<sup>34</sup> Nevertheless, some characteristic differences are observed between the Raman spectra of the  $\alpha$ -HQ and the

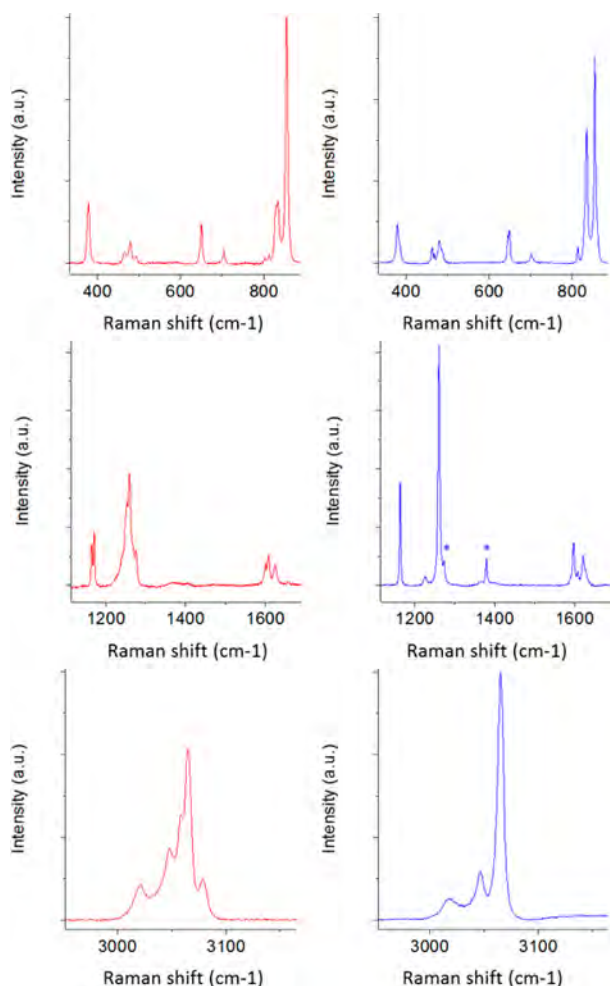


**Figure 3.** Raman spectra of  $\alpha$ -HQ (in red) and  $\text{CO}_2$ -HQ clathrate (in blue) for Raman shift ranging from 350 to 3300  $\text{cm}^{-1}$ . The asterisk \* shows the characteristic Raman band of  $\text{CO}_2$  guest molecules at 1272 and 1380  $\text{cm}^{-1}$ .

$\text{CO}_2$ -HQ clathrate. We have noticed that the C-H stretching band, at 3080  $\text{cm}^{-1}$  in  $\alpha$ -HQ, is absent in the  $\text{CO}_2$ -HQ clathrate form, in good agreement with the calculations of Kubinyi et al.<sup>32</sup> In addition, the bands close to 480 and 850  $\text{cm}^{-1}$ , and the group of three bands at 1599, 1610, and 1623  $\text{cm}^{-1}$ , attributed to C-C stretching modes of the HQ molecules, show clear variation in relative band intensities between the two forms. Our results are in agreement with those obtained previously by Park et al.,<sup>35</sup> who have found 1601, 1611, and 1625  $\text{cm}^{-1}$  for this group of bands. The two C-H bending bands at 1163 and 1169  $\text{cm}^{-1}$  in the spectra of  $\alpha$ -HQ appear as a single band at 1163  $\text{cm}^{-1}$  in the spectra of our clathrate sample. The bands centered at 1257  $\text{cm}^{-1}$  in the spectra of  $\alpha$ -HQ, due to coupled C-O and C-C stretching modes are shifted to higher frequency (1260  $\text{cm}^{-1}$ ) in the spectra of the  $\text{CO}_2$ -HQ clathrate.<sup>32,36</sup>

In the IR spectra, Figure 4, the characteristic bands of  $\alpha$ -HQ are at first sight invariant in the  $\text{CO}_2$ -HQ clathrate, but there are minor differences between the spectra, such as some changes in relative intensities of the bands close to 1350 and 1600  $\text{cm}^{-1}$ , due to three nonequivalent HQ molecules in the asymmetric unit cell of the  $\alpha$ -form.<sup>10,31</sup> Moreover, the frequency of the OH bending band at 1228  $\text{cm}^{-1}$  in Raman spectrum (Figure 3) and the broadening of the  $\nu$ -OH

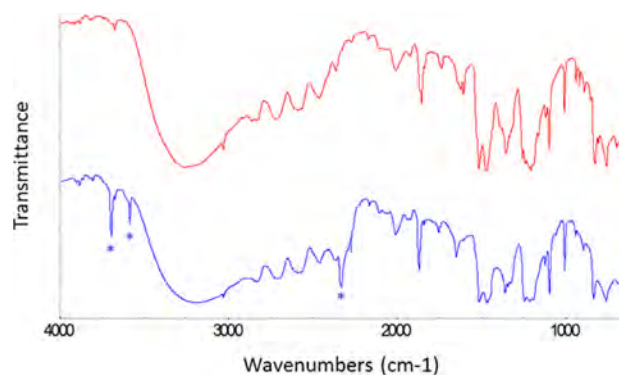


**Figure 4.** IR spectra of  $\alpha$ -HQ (in red) and  $\text{CO}_2$ -HQ clathrate (in blue). The asterisk \* shows the signature of the  $\text{CO}_2$  at 2335, 3588, and 3695  $\text{cm}^{-1}$ .

stretching band (characteristic of intermolecular hydrogen bonds) around 3160  $\text{cm}^{-1}$  in the FT-IR spectrum (Figure 4) clearly show that the hydrogen bonding organic framework (HOF) is altered between the two HQ forms and that the clathrate form has a more symmetrical structure than the  $\alpha$ -HQ.<sup>32,37</sup> Concerning the guest  $\text{CO}_2$  molecule, the Fermi resonance doublet of the symmetrical C=O stretch and the antisymmetric C=O stretch have been observed at 1272 and 1380  $\text{cm}^{-1}$  in the Raman spectrum (see Figure 3) and 2335  $\text{cm}^{-1}$  in the FT-IR spectrum (see Figure 4), respectively. As reported in the literature,<sup>38</sup> two combinations bands are also observed at 3588 and 3695  $\text{cm}^{-1}$  in the FT-IR spectrum. Thus, we deduce that the centrosymmetric structure of the  $\text{CO}_2$  guest is retained in the HQ host lattice.<sup>31</sup> It is worth noting that the signature observed in IR and Raman spectroscopy for the  $\text{CO}_2$  in gaseous phase are slightly different from that of the  $\text{CO}_2$  in the clathrate. For the  $\text{CO}_2$  gas, our FT-IR spectrum exhibits three double bands at 2341 and 2360, 3599 and 3625, 3704, and 3729  $\text{cm}^{-1}$  as reported in the literature.<sup>39</sup> In Raman spectroscopy, we found the Fermi dyad for  $\text{CO}_2$  gas at 1287 and 1390  $\text{cm}^{-1}$  and hot bands at 1267 and 1411  $\text{cm}^{-1}$ . For the  $\text{CO}_2$ -HQ clathrate, we observed only three bands at 2335, 3588, and 3695  $\text{cm}^{-1}$  in FT-IR, and two Raman bands (shifted compared to those of  $\text{CO}_2$  gas) at 1272 and 1380  $\text{cm}^{-1}$ . The differences between the IR and Raman spectroscopic signatures of  $\text{CO}_2$  in the gas and in the clathrate (shift toward lower frequencies) are principally ascribed both to the presence of host-guest interactions and to the spatial constraints of the  $\text{CO}_2$  molecules encapsulated in the clathrate lattice, as already pointed out for other inclusion compounds such as gas hydrates.<sup>40</sup>

Figure 5 shows the  $^{13}\text{C}$  NMR analysis.

Two groups of signals (five singlets at about 116 ppm and three singlets at about 148 ppm) were observed for pure  $\alpha$ -HQ before the reaction with  $\text{CO}_2$ . These signals correspond to the two different carbon atoms in HQ molecules: one for the hydroxyl-substituted carbon atoms at 148 ppm and the other for the C-H carbon atoms at 116 ppm.<sup>33</sup>

After the reaction of HQ with  $\text{CO}_2$ , the NMR spectrum shows three distinct signals, which represent three inequivalent carbon atoms of the HQ molecules in the HQ clathrate framework.<sup>41</sup> The chemical shift of the peak corresponding to the carbon atoms attached to the hydroxyl group is 148.2 ppm. The signals for the C-H carbon atoms appear at 117.8 and 115.2 ppm, respectively. The chemical shift of  $\text{CO}_2$  molecules encapsulated in the HQ host framework is clearly observed at

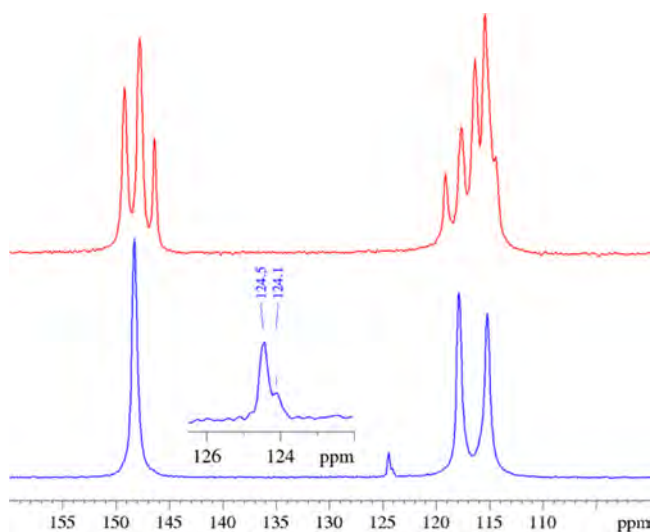


**Figure 5.**  $^{13}\text{C}$  NMR spectra of  $\alpha$ -HQ (in red) and  $\text{CO}_2$ -HQ clathrate (in blue). The enlargement shows the signals of  $\text{CO}_2$  molecules enclosed in the HQ clathrate.

124 ppm. Interestingly, the NMR signal of  $\text{CO}_2$  enclathrated in the HQ host lattice exhibits two peaks with chemical shifts relatively close to each other (124.0 and 124.5 ppm), showing that two different chemical environments exist for the  $\text{CO}_2$  molecule in the clathrate structure. The guests molecules present in such clathrates, and particularly  $\text{CO}_2$ , are supposed to interact with one another from cage to cage.<sup>42</sup> This double  $\text{CO}_2$  peak could result from the heterogeneity of guest-guest interactions as empty cages are also present in the structure (a given  $\text{CO}_2$  molecule located in a cage can either interact with another  $\text{CO}_2$  molecule located in the upper/lower cage, or not if this adjacent cage is empty). Integration of the  $\text{CO}_2$  peaks gives a surface ratio of 74.8/25.2 for the peaks at 124.5 and 124.0 ppm, respectively. Because of the complex nature of the guest-guest interaction, and without the information on how the empty cages are distributed inside the clathrate structure, we are not able for the moment to correlate this peak ratio value with the clathrate formula. This would require complementary studies, such as periodic quantum chemistry calculations or statistical analysis, which are currently under investigation in our laboratory.

All the results obtained using spectroscopy techniques (i.e., Raman, IR, and NMR) demonstrate that the crystals formed during the synthesis are HQ clathrate containing  $\text{CO}_2$  as a guest and that the  $\text{CO}_2$ -HQ clathrate crystals isolated at the end of the purification step are of very high purity (no trace of impurities, such as  $\alpha$ -HQ, detected with respect to the limit of detection of the apparatuses and analytical methods used).

**Morphology of the Crystals.** This section concerns the visualization of the clathrate using an optical microscope under ambient conditions. The most interesting views are shown and compared with the morphology of the native  $\alpha$ -HQ crystals (used as raw material for the synthesis) in Figure 6.

Both  $\alpha$ -HQ and the clathrate grew as needles.  $\alpha$ -HQ crystals were obtained as  $\sim 100$ – $200\ \mu\text{m}$  long needles (inset Figure 6a), with well-developed, smooth facets (Figure 6c). The clathrate needles were quite different. First, they were an order of magnitude longer and broader (Figure 6a). Furthermore, their lateral faces were predominantly rounded, with rare facets. Completely different from the  $\alpha$ -HQ, the clathrate surface

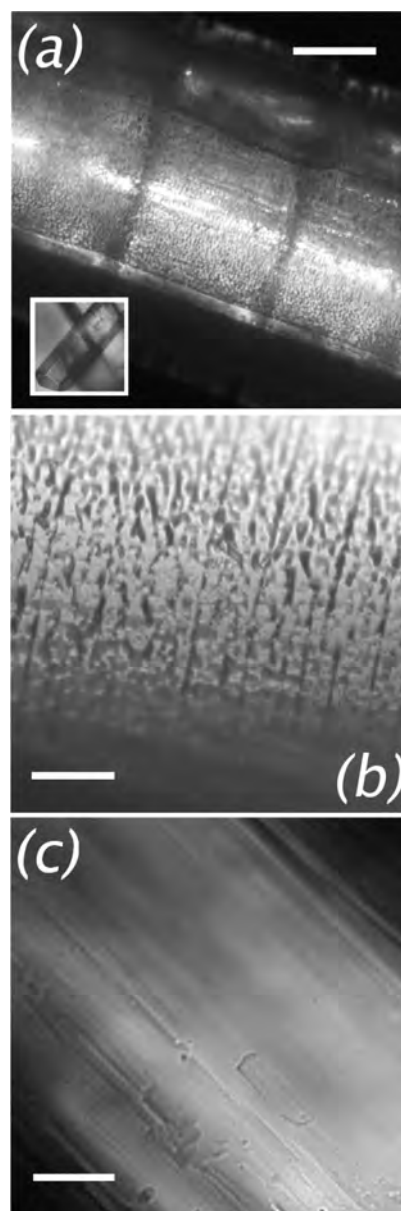


**Figure 6.** Optical transmission micrographs. Clathrate crystals are larger, more rounded, and rougher than the host crystal: (a) Side view of a  $\text{CO}_2$ -HQ needle (inset: the pure host,  $\alpha$ -HQ, at the same scale); (b, c) close up views of the clathrate and  $\alpha$ -HQ surfaces, respectively. Scale bars: (a)  $100\ \mu\text{m}$ ; (b–c)  $20\ \mu\text{m}$ .

exhibited  $\sim 2\ \mu\text{m} \times \sim 10\ \mu\text{m}$  pores emerging from the crystal bulk, aligned with their longer dimension perpendicular to the needle axis (cf, Figure 6, panels b and c). The pore walls were some microns thick. Light scattering by this microstructure explains the opacity of the crystals noted above. Besides the pore structure, the clathrate was seen to be segmented at one and sometimes two scales. The smaller was the presence of more or less continuous circumferential clefts,  $\sim <1\ \mu\text{m}$  wide, perpendicular to the needle axis (Figure 6b). The clefts were spaced  $10$ – $20\ \mu\text{m}$  apart. The second scale was observed on many but not all crystals as the presence of dark rings,  $\sim 10\ \mu\text{m}$  wide, spaced  $150$ – $200\ \mu\text{m}$  apart (Figure 6a). These rings did not interrupt the local texture of the surface.

**Thermal Response and Clathrate Occupancy.**  $\alpha$ -HQ and  $\text{CO}_2$ -HQ clathrate were analyzed by TGA/SM. Figure 7

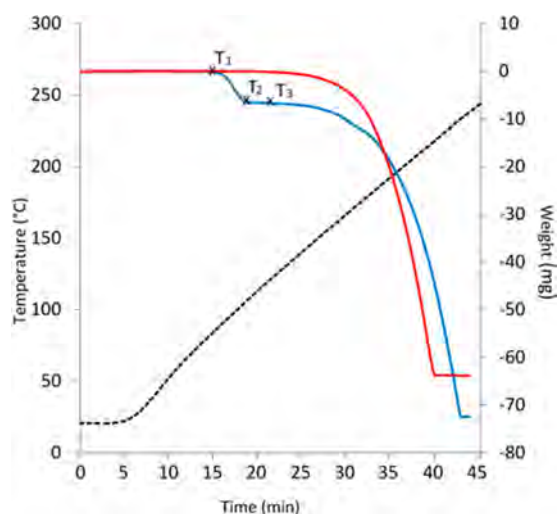


**Figure 7.** TGA thermograms showing the evolution of the sample weight during a temperature ramp.  $\alpha$ -HQ (in red),  $\text{CO}_2$ -HQ clathrate (in blue), and temperature ramp (dashed line).

compares the evolution of the sample weight when submitted to a temperature ramp. The degree of repeatability is good and was checked from several measurements on two samples obtained under the same conditions of synthesis.

The first signal “jump” (from  $T_1$  to  $T_2$ ) shown on the thermogram displayed in Figure 7 corresponds to the release of  $\text{CO}_2$  by the  $\text{CO}_2$ -HQ clathrate. This process starts to be noticeable at  $T_1 \approx 80^\circ\text{C}$  and ends at around  $T_2 \approx 110^\circ\text{C}$ . Note that a single value of this decomposition temperature was indicated by McAdie at respectively 101.1 and  $103.3^\circ\text{C}$  from DTA analyses carried out on  $\text{CO}_2$ -HQ clathrates in static and dynamic conditions.<sup>43,44</sup> The presence of  $\text{CO}_2$  only during the first weight loss is confirmed by mass spectrum analysis (see Figure 8). In fact, all charged fragments were present in the recorded mass spectrum (44, 28, 16, 12) during this period. However, to clarify the figure, only the pattern fragment was shown in Figure 8.

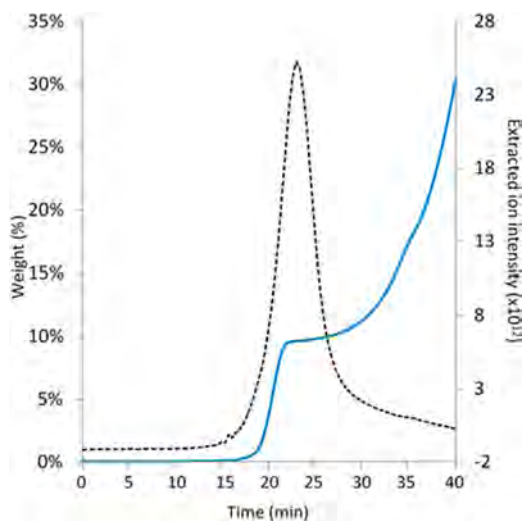


**Figure 8.** Evolution of the percentage of weight loss of a  $\text{CO}_2$ -HQ clathrate sample (continuous blue line), coupled to mass spectrum signal ( $\text{CO}_2$  pattern fragment, black dashed line).

A second decomposition stage, occurring between  $T_3 \approx 120^\circ\text{C}$  and around  $225^\circ\text{C}$ , is attributed to HQ sublimation, as hydroquinone is known to sublime readily at temperatures much lower than its melting point ( $\sim 170^\circ\text{C}$ ).<sup>5,45</sup>

Interestingly, as seen in Figure 7, sublimation of  $\alpha$ -HQ is started at a slightly lower temperature than measured for the  $\text{CO}_2$ -HQ clathrate. In contrast, we can see that  $\alpha$ -HQ sublimates faster than  $\text{CO}_2$ -HQ clathrate.

Concerning the thermal properties of the crystals and the quantity of  $\text{CO}_2$  enclathrated, we can see in Figure 8 that the total  $\text{CO}_2$  stored in these crystals was up to 8.9 wt % corresponding to a clathrate occupancy of about 71% in these conditions, or a clathrate formula of  $0.71 \text{CO}_2\text{-}3\text{HQ}$ . Although the clathrate formation conditions are different, our result is in agreement with published values  $\sim 74\%$  for  $\text{CO}_2$ -HQ clathrates obtained by crystallization in a solvent.<sup>5,25,44</sup> The largest value for this system (about 75%) was found by Peyronel and Barbieri.<sup>29</sup>

An additional experiment was performed to estimate the stability of the  $\text{CO}_2$ -HQ clathrate stored at ambient conditions (atmospheric pressure, temperature of  $25 \pm 2^\circ\text{C}$ ). Note that in these conditions, this compound is out of its thermodynamical stability region, as the triphasic equilibrium point at  $25^\circ\text{C}$  (i.e., the point where the  $\text{HQ}_{\text{cr}}$ , the  $\text{CO}_2$ -HQ clathrate, and the  $\text{CO}_2$  gas coexists at  $25^\circ\text{C}$ ) has been measured at  $0.84 \pm 0.15$  bar of  $\text{CO}_2$ .<sup>27</sup> Thus, from a new synthesis of  $\text{CO}_2$ -HQ clathrate, the crystals obtained were stored in a glass flask, kept for 14 days out of direct sunlight, at ambient conditions. Using TGA, the crystals were first analyzed immediately after the end of the synthesis (this time is denoted  $t_0$ ) and then at different times ( $t_0 + 3$  days,  $t_0 + 10$  days, and  $t_0 + 14$  days). The results obtained have been found independent of the TGA heating rate ( $5^\circ\text{C}\cdot\text{min}^{-1}$  and  $2^\circ\text{C}\cdot\text{min}^{-1}$ ). As shown in Figure 9, the

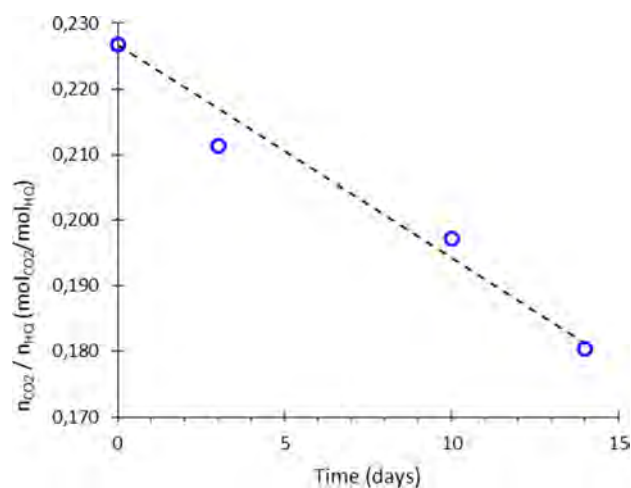


**Figure 9.** Evolution of the molar quantity of  $\text{CO}_2$  per mole of HQ versus time for  $\text{CO}_2$ -HQ clathrate crystals stored at ambient conditions, measured by TGA with a heating rate of  $5^\circ\text{C}\cdot\text{min}^{-1}$ .

evolution of the molar ratio  $n_{\text{CO}_2}/n_{\text{HQ}}$  versus time demonstrates clearly that the  $\text{CO}_2$  slowly escapes the clathrate structure, leading to progressively decrease the clathrate occupancy from  $x = 0.68$  (at  $t_0$ ) to  $x = 0.54$  (at  $t_0 + 14$  days). From this experiment, the  $\text{CO}_2$  degassing rate has been estimated at  $3.25 \text{mmol}_{\text{CO}_2}\cdot\text{mol}_{\text{HQ}}^{-1}\cdot\text{day}^{-1}$  (obtained by linear regression of the four data points). Therefore, in light of these results, the  $\text{CO}_2$ -

HQ clathrate at ambient conditions can be considered as a *relatively stable* structure in time. However, the crystals should be analyzed as quickly as possible after the end of the synthesis to obtain reliable quantitative analyses, and if several analyses have to be done to obtain crossed results, they must be performed at the same time (such as done in this study).

**Crystal Structure of the CO<sub>2</sub>-HQ Clathrate.** Some molecular structures of HQ clathrates have already been published in the literature, such as those of xenon,<sup>46</sup> nitric oxide,<sup>47</sup> hydrogen sulfide,<sup>48</sup> and hydrogen chloride.<sup>49</sup> However, the molecular structure of HQ clathrate formed with carbon dioxide has not been described to date. The only experimental structural data we have to date for the CO<sub>2</sub>-HQ clathrate are the structural lattice parameters obtained by Palin and Powell in 1947.<sup>50</sup> In the light of both the recently highlighted, potential practical applications of CO<sub>2</sub>-HQ and the necessity to increase our fundamental knowledge on this compound, the molecular structure of the CO<sub>2</sub>-HQ clathrate is of paramount importance. These data are an important outcome of this study. The influence of temperature on this structure and the molecular structure of the CO<sub>2</sub>-HQ clathrate are presented.

The experimental apparatus and method used to perform XRD analysis are described in the [Supporting Information](#) (SI). The temperature effect on the structure measured at different temperatures (233, 173, and 100 K) is nicely illustrated in [Figure 10](#). The size of the ellipsoids, especially concerning the

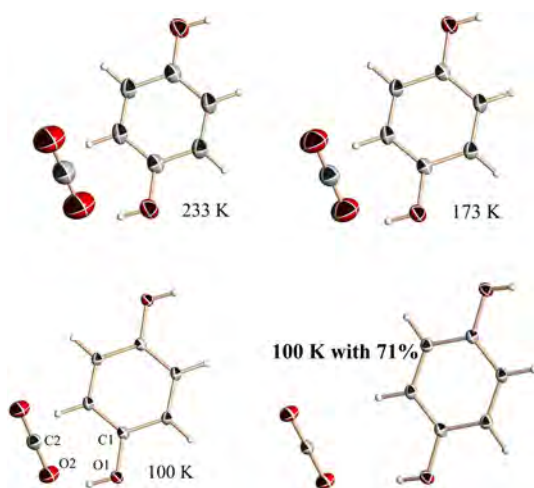


**Figure 10.** Molecular structures of the HQ and CO<sub>2</sub> molecules measured at different temperatures illustrating the temperature effect on the thermal ellipsoids depicted at the 50% level. Selected bond lengths [Å]: for 233 K: C1-O1 = 1.340(2), C2-O2 = 1.144(4); for 173 K: C1-O1 = 1.379(2), C2-O2 = 1.146(3); for 100 K: C1-O1 = 1.380(1), C2-O2 = 1.155(2), for 100 K with 71%: C1-O1 = 1.382(2), C2-O2 = 1.157(2).

invited CO<sub>2</sub> molecule, depends naturally on the measuring temperature and on possible disorder of the molecules. The small ellipsoids of the invited molecule reflect the perfect localization of the CO<sub>2</sub> in the host lattice. Another important point is that the clathrate occupancy is about 71% in our case, found by TGA. We calculated the occupancy of the CO<sub>2</sub> molecule by structure analysis and the value refined to about 87% for the 100 K measurement (see [Figure 10](#)). While higher than the value from TGA, this figure is strongly correlated to the thermal ellipsoids. The CO<sub>2</sub> molecule is not really fixed in the cavity, so we could expect an overestimation, and in this

particular case crystallography gives only an idea but not an accurate value for this occupancy. By fixing the occupancy of CO<sub>2</sub> to 71% in the structure model, the thermal ellipsoids become nearly perfect in comparison to the host molecule, but the *R* value increases from 0.0362 (for all data with 87% occupancy) to 0.0442 (for all data with 71% occupancy). Probably the real occupancy lies between these values.

The arrangement of the host molecules in the space group  $R\bar{3}$  is in perfect agreement with HQ clathrate structure (see [Figure 11](#)). The HQ molecules are on inversion centers located

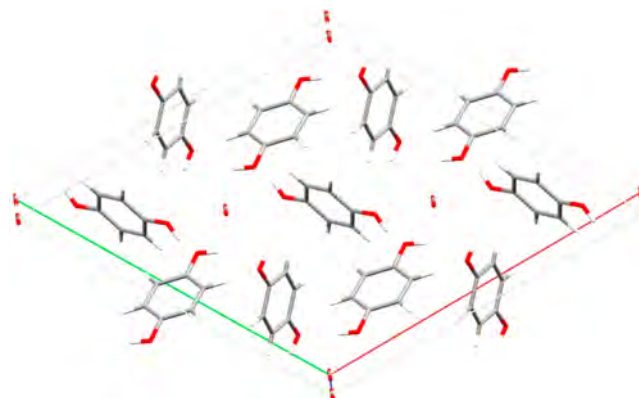


**Figure 11.** Arrangement of the HQ and CO<sub>2</sub> molecules in the solid state. This view is the unit cell tilted off the *c* axis.

in the middle of the aromatic ring systems. Only half of the molecule is in the asymmetric unit, the other moiety is generated by the inversion center. The CO<sub>2</sub> molecules lie on the *c* axis, on 3-fold rotainversion axes. Moreover, the carbon atom of the CO<sub>2</sub> is on an inversion center, so only a sixth of the carbon atom and a third of the oxygen atom are in the asymmetric unit.

As discussed in the [Introduction](#), six hydroquinone molecules form a cage by hydrogen bonds (see [Figure 12](#)). Each HQ molecule takes part in two cages involving the two OH groups. In order to evaluate the intermolecular interactions, all hydrogen atoms of this structure have been located by difference-Fourier map, and the positions have been refined freely by fixing the isotropic temperature factors to 1.5 times for the OH and 1.2 times for the aromatic hydrogen atoms relative to the temperature factors of the bonded O and C atoms, respectively. The O...O distance of the hydrogen bonds between the HQ molecules, 2.68 Å, is in perfect agreement with literature values for O-H...O hydrogen bonds (2.50–2.80 Å).<sup>51</sup> No hydrogen-bonding interactions between the host and the guest molecules could be observed.

Another often discussed parameter concerns the angle  $\theta$  between the plane formed by the six oxygen atoms joined by hydrogen bonds and the axis of the O-C<sub>1</sub>...C<sub>4</sub>-O of the HQ unit (i.e., the tilt of the HQ molecular axis of the *ab* plane). We find  $\theta = 44.7^\circ$ , close to estimated values for this compound.<sup>5</sup> Palin and Powell calculated this angle  $\theta$  for a series of HQ clathrates with different guest molecules.<sup>5</sup> This estimation was based on geometrical calculations using the cell parameters by fixing the length of the HQ molecule (O-C<sub>6</sub>H<sub>4</sub>-O distance = 5.50 Å) and the distance *d* between the center of the six-membered O<sub>6</sub> ring system formed by hydrogen bonds and the oxygen atoms involved (*d* = 2.75 Å). In the case of CO<sub>2</sub> they noted a problem, because using the cell parameters *a* or *c* leads to different values for  $\theta$ , 45.78° and 44.87°, respectively. They



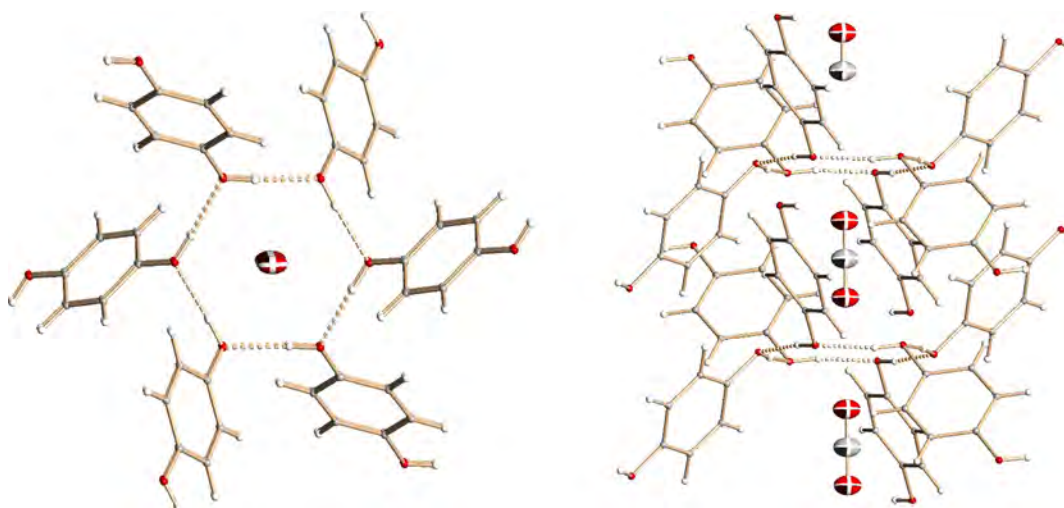


**Figure 12.** Illustration of the cage arrangement. HQ molecules have been simplified for clarity. The view along the CO<sub>2</sub> molecules (left) shows the hexagonal arrangement formed by hydrogen-bonds between OH groups. The side-view of the cage is shown on the right.

supposed that this problem could be solved by using  $d < 2.72$  Å, meaning that the hydrogen bonds are stronger than expected in the CO<sub>2</sub>-HQ clathrate. Indeed, our experimental value is  $d = 2.68$  Å, and the experimental length of the HQ molecule is 5.54 Å.

Another important point concerns the fact that the clathrate occupancy is about 71% in our case, found by TGA. We calculated the occupancy of the CO<sub>2</sub> molecule also by structure analysis and the value refined to about 87%. This seems to be high with respect to the TGA, but this value is strongly correlated to the thermal ellipsoids, and the CO<sub>2</sub> molecule is not really fixed in the cavity, so we could expect an overestimation, and in this particular case crystallography gives only an idea but not an accurate value for this occupancy.

The supplementary crystallographic data can be obtained free of charge from The Cambridge Crystallographic Data Centre via [www.ccdc.cam.ac.uk/data\\_request/cif](http://www.ccdc.cam.ac.uk/data_request/cif), with the accession codes CCDC-1482725, CCDC-1482726, CCDC-1482727, and CCDC-1482726.

## CONCLUSION

Fundamental science and applications call for an in-depth investigation of the CO<sub>2</sub>-HQ clathrate compound. For example, the lack of precise data on the spatial arrangement of the atoms is detrimental to theoretical investigations that could be made in the near future, such as molecular dynamics simulations, thermodynamical modeling, and quantum chemistry calculations. CO<sub>2</sub>-HQ clathrate is moreover one of the key structures of many applications such as gas storage and gas separation by selective clathration.

This study presented a novel synthesis and purification of CO<sub>2</sub>-HQ monocrystals. The protocol used allowed forming at constant temperature (25 °C) and visualizing the growth of the crystal under pressure, under 30 bar of CO<sub>2</sub> and using ethanol as the solvent. Two steps contribute to isolating the clathrate crystals: the purification step, consisting of first washing the crystals obtained with CH<sub>2</sub>Cl<sub>2</sub>, and the separation of the clathrate form ( $\beta$ -form) from the remaining native HQ structure ( $\alpha$ -form) by density difference.

These crystals have then been characterized by spectroscopy techniques such as Raman, infrared, and <sup>13</sup>C NMR. The collection of spectra presented here provides a complete set of

data on this compound. All the spectroscopic analyses have demonstrated that the purified crystals are pure CO<sub>2</sub>-HQ clathrate. The morphologies of the  $\alpha$  and  $\beta$  forms were also visualized by optical microscopy and revealed unreported features. While  $\alpha$ -HQ crystals exhibit a smooth surface aspect, the clathrate crystals are needles with a porous structure. Thermal differential analysis coupled to mass spectroscopy allowed both determining the thermal response of the compound and obtaining the quantity of gas encapsulated in this clathrate, i.e., the clathrate occupancy. When the crystal is submitted to a temperature ramp at atmospheric pressure, it was shown that the CO<sub>2</sub> was liberated at a temperature close to 80 °C. The clathrate occupancy implies the clathrate formula 0.71 CO<sub>2</sub>-3HQ. Data on clathrate occupancy versus time for CO<sub>2</sub>-HQ clathrate crystals stored 14 days at ambient conditions demonstrate that this compound is relatively stable in time, even if these conditions are outside the region of thermodynamical stability: the CO<sub>2</sub> slowly escapes from the clathrate structure, leading to a decrease of the clathrate occupancy of about 1% per day.

Finally, the crystal structure of the CO<sub>2</sub>-HQ clathrate was obtained by XRD analysis at three temperatures. The results obtained at 100 K confirm that this clathrate has a distorted cavity and reflect a perfect localization of the CO<sub>2</sub> in the host lattice. The CO<sub>2</sub> molecules encapsulated in the clathrate are perfectly aligned to one another and are placed along direction  $c$  on 3-fold rotainversion axes of the structure. The symmetry group of this clathrate is then  $R\bar{3}$ ; i.e., CO<sub>2</sub> forms a type I clathrate with HQ following Powell's structure classification.

As a matter of fact, much remains poorly or not at all understood for organic clathrates of gases. The study of these compounds, which have been much less studied than other inclusion compounds such as gas hydrates, for example, opens interesting routes for future theoretical work and novel crystal engineering applications.

## ASSOCIATED CONTENT

### Supporting Information

The Supporting Information is available free of charge on the ACS Publications website at DOI: 10.1021/acs.cgd.6b00834.

Experimental apparatus used for the synthesis, characterization apparatuses and methods, materials (PDF)

## Accession Codes

CCDC 1482725–1482726 and 1482726–1482727 contain the supplementary crystallographic data for this paper. These data can be obtained free of charge via [www.ccdc.cam.ac.uk/data\\_request/cif](http://www.ccdc.cam.ac.uk/data_request/cif), or by emailing [data\\_request@ccdc.cam.ac.uk](mailto:data_request@ccdc.cam.ac.uk), or by contacting The Cambridge Crystallographic Data Centre, 12 Union Road, Cambridge CB2 1EZ, UK; fax: +44 1223 336033.

## AUTHOR INFORMATION

### Corresponding Author

\*Phone: +33(0)5 40 17 51 09. Fax: +33(0)5 79 40 77 25. E-mail: [jean-philippe.torre@univ-pau.fr](mailto:jean-philippe.torre@univ-pau.fr).

### Notes

The authors declare no competing financial interest.

## ACKNOWLEDGMENTS

The CNRS (Centre National de la Recherche Scientifique) and the Institute Carnot ISiFoR (Institute for the Sustainable engineering of Fossil Resources) are acknowledged for supporting this work. Joseph Diaz, Fabrice Guerton, and Jean-Paul Grenet are also thanked for their assistance with the experimental apparatus.

## REFERENCES

- (1) Dyadin, Yu. A.; Terekhova, I. S. In *Encyclopedia of Supramolecular Chemistry*; Atwood, J. L., Steed, J. W., Eds.; CRC Press, Taylor & Francis Group: Boca Raton, FL, 2004; Vol. 1, pp 253, 260.
- (2) MacNicol, D. D. In *Inclusions Compounds: Structural Aspects of Inclusion Compounds Formed by Organic Host Lattices*; Atwood, J. L., Davies, J. E. D., MacNicol, D. D., Eds.; Academic Press Inc.: London, 1984; Vol. 2, Chapter 1, pp 1–45.
- (3) Naoki, M.; Yoshizawa, T.; Fukushima, N.; Ogiso, M.; Yoshino, M. *J. Phys. Chem. B* **1999**, *103*, 6309–6313.
- (4) Powell, H. M. *J. Chem. Soc.* **1948**, 61–73.
- (5) Palin, D. E.; Powell, H. M. *J. Chem. Soc.* **1948**, 0, 815–821.
- (6) Birchall, T.; Frampton, C. S.; Schrobilgen, G. J.; Valsdottir, J. *Acta Crystallogr., Sect. C: Cryst. Struct. Commun.* **1989**, *45*, 944–946. [10.1107/S0108270188014556](https://doi.org/10.1107/S0108270188014556)
- (7) Mak, T. C. W.; Lee, K.-S. *Acta Crystallogr., Sect. B: Struct. Crystallogr. Cryst. Chem.* **1978**, *34*, 3631–3634.
- (8) Mak, T. C. W.; Lam, C.-K. In *Encyclopedia of Supramolecular Chemistry*; Atwood, J. L., Steed, J. W., Eds.; CRC Press, Taylor & Francis Group: Boca Raton, FL, 2004; Vol. 1, pp 679, 686.
- (9) Chan, T.-L.; Mak, T. C. W. *J. Chem. Soc., Perkin Trans. 2* **1983**, *6*, 777–781.
- (10) Wallwork, S. C.; Powell, H. M. *J. Chem. Soc., Perkin Trans. 2* **1980**, *2*, 641–646.
- (11) Marsh, R. E. *Acta Crystallogr., Sect. B: Struct. Sci.* **2002**, *58*, 893–899.
- (12) Powell, H. M. *J. Chem. Soc.* **1950**, 298–300.
- (13) Yoon, J. H.; Lee, Y. J.; Park, J.; Kawamura, T.; Yamamoto, Y.; Komai, T.; Takeya, S.; Han, S. S.; Lee, J. W.; Lee, Y. *ChemPhysChem* **2009**, *10*, 352–355.
- (14) Maartmann-Moe, K. *Acta Crystallogr.* **1966**, *21*, 979–982.
- (15) Andersson, K.; Nakazawa, Y. *Curr. Inorg. Chem.* **2014**, *4*, 2–18.
- (16) Chleck, D. J.; Ziegler, C. A. *Int. J. Appl. Radiat. Isot.* **1959**, *7*, 141–144.
- (17) Han, K. W.; Lee, Y.-J.; Jang, J. S.; Jeon, T.-I.; Park, J.; Kawamura, T.; Yamamoto, Y.; Sugahara, T.; Vogt, T.; Lee, J.-W.; Lee, Y.; Yoon, J.-H. *Chem. Phys. Lett.* **2012**, *546*, 120–124.
- (18) Rozsa, V. F.; Strobel, T. A. *J. Phys. Chem. Lett.* **2014**, *5*, 1880–1884.
- (19) Lee, J.-W.; Kang, S.-P.; Yoon, J.-H. *J. Phys. Chem. C* **2014**, *118*, 7705–7709.
- (20) Lee, J.-W.; Kang, S.-P.; Yoon, J.-H. *J. Phys. Chem. C* **2014**, *118*, 6059–6063.
- (21) Leung, D. Y. C.; Caramanna, G.; Maroto-Valer, M. M. *Renewable Sustainable Energy Rev.* **2014**, *39*, 426–443.
- (22) McDonald, T. M.; Mason, J. A.; Kong, X.; Bloch, E. D.; Gygi, D.; Dani, A.; Crocellà, V.; Giordanino, F.; Odoh, S. O.; Drisdell, W. S.; Vlaisavljevich, B.; Dzubak, A. L.; Poloni, R.; Schnell, S. K.; Planas, N.; Lee, K.; Pascal, T.; Wan, L. F.; Prendergast, D.; Neaton, J. B.; Smit, B.; Kortright, J. B.; Gagliardi, L.; Bordiga, S.; Reimer, J. A.; Long, J. R. *Nature* **2015**, *519*, 303–308.
- (23) Lee, J.-W.; Yoon, J.-H. *J. Phys. Chem. C* **2011**, *115*, 22647–22651.
- (24) Lee, J.-W.; Dotel, P.; Park, J.; Yoon, J.-H. *Korean J. Chem. Eng.* **2015**, *32*, 2507–2511.
- (25) Lee, Y.-J.; Han, K. W.; Jang, J. S.; Jeon, T.-I.; Park, J.; Kawamura, T.; Yamamoto, Y.; Sugahara, T.; Vogt, T.; Lee, J.-W.; et al. *ChemPhysChem* **2011**, *12*, 1056–1059.
- (26) Conde, M. M.; Torrè, J.-P.; Miquieu, C. *Phys. Chem. Chem. Phys.* **2016**, *18*, 10018–10027.
- (27) Coupán, R.; Chabod, M.; Dicharry, C.; Diaz, J.; Miquieu, C.; Torrè, J.-P. *J. Chem. Eng. Data* **2016**, *61*, 2565–2572.
- (28) Mandelcorn, L. *Chem. Rev.* **1959**, *59*, 827–839.
- (29) Peyronel, G.; Barbieri, G. *J. Inorg. Nucl. Chem.* **1958**, *8*, 582–585.
- (30) Li, X.; Chen, Q. Y.; Wang, J. *J. Chem. Eng. Data* **2006**, *51*, 127–129.
- (31) Davies, J. E. D. *J. Chem. Soc., Dalton Trans.* **1972**, *11*, 1182–1188.
- (32) Kubinyi, M. J.; Keresztury, G. *Mikrochim. Acta* **1997**, *14*, 525–528.
- (33) Lee, J.-W.; Choi, K. J.; Lee, Y.; Yoon, J.-H. *Chem. Phys. Lett.* **2012**, *528*, 34–38.
- (34) Ilczyszyn, M.; Selent, M.; Ilczyszyn, M. M.; Baran, J. *Vib. Spectrosc.* **2011**, *55*, 107–114.
- (35) Park, J.-W.; An, S.; Seo, Y.; Kim, B.-S.; Yoon, J.-H. *J. Phys. Chem. C* **2013**, *117*, 7623–7627.
- (36) Jakobsen, R. J.; Brewer, E. J. *Appl. Spectrosc.* **1962**, *16*, 32–35.
- (37) Lee, J.-W.; Lee, Y.; Takeya, S.; Kawamura, T.; Yamamoto, Y.; Lee, Y.-J.; Yoon, J.-H. *J. Phys. Chem. B* **2010**, *114*, 3254–3258.
- (38) Sandford, S. A.; Allamandola, L. J. *Astrophys. J.* **1990**, *355*, 357–372.
- (39) Oancea, A.; Grasset, O.; Le Menn, E.; Bollengier, O.; Bezacier, L.; Le Mouélic, S.; Tobie, G. *Icarus* **2012**, *221*, 900–910.
- (40) Nakano, S.; Moritoki, M.; Ohgaki, K. *J. Chem. Eng. Data* **1998**, *43*, 807–810.
- (41) Ripmeester, J. A. Application of Solid state <sup>13</sup>C NMR to the study of polymorphs, clathrates and complexes. *Chem. Phys. Lett.* **1980**, *74*, 536–538.
- (42) Zubkus, V. E.; Tornau, E. E.; Belosludov, V. R. *Adv. Chem. Phys.* **1991**, *81*, 269–359.
- (43) McAdie, H. G. *Can. J. Chem.* **1963**, *41*, 2137–2143.
- (44) McAdie, H. G. *Can. J. Chem.* **1966**, *44*, 1373–1385.
- (45) Coutant, R. W. *J. Org. Chem.* **1974**, *39*, 1593–1594.
- (46) Ilczyszyn, M.; Selent, M.; Ilczyszyn, M. M. *J. Phys. Chem. A* **2012**, *116*, 3206–3214.
- (47) Arulsamy, N.; Bohle, D. S.; Butikofer, J. L.; Stephens, P. W.; Yee, G. T. *Chem. Commun.* **2004**, 1856–1857.
- (48) Ho, W. C.; Mak, T. C. W. *Z. Kristallogr., Kristallgeom., Kristallphys., Kristallchem.* **1982**, *161*, 87–90.
- (49) Boeyens, J. C. A.; Pretorius, J. A. *Acta Crystallogr., Sect. B: Struct. Crystallogr. Cryst. Chem.* **1977**, *33*, 2120–2124.
- (50) Palin, D. E.; Powell, H. M. *J. Chem. Soc.* **1947**, 208–221.
- (51) Pauling, L. In *The Nature of the Chemical Bond*, 3rd ed.; Cornell University Press: Ithaca, NY, 1960; Chapter 12, pp 484–485.

## SUPPORTING INFORMATION

# CO<sub>2</sub> – Hydroquinone Clathrate: Synthesis, Purification, Characterization and Crystal Structure

*Jean-Philippe TORRÉ<sup>1,\*</sup>, Romuald COUPAN<sup>1</sup>, Mathieu CHABOD<sup>1</sup>, Eve PERE<sup>2</sup>, Stéphane LABAT<sup>2</sup>, Abdel KHOUKH<sup>2</sup>, Ross BROWN<sup>2</sup>, Jean-Marc SOTIROPOULOS<sup>2</sup>, Heinz GORNITZKA<sup>3,4</sup>*

<sup>1</sup>. Université Pau & Pays Adour. Laboratoire des Fluides Complexes et leurs Réservoirs (LFCR), UMR CNRS 5150, Avenue de l'Université, BP 1155, F-64013, Pau, France

<sup>2</sup>. Université Pau & Pays Adour. Institut des Sciences Analytiques et de Physico-Chimie pour l'Environnement et les Matériaux (IPREM), UMR CNRS 5254. Hélioparc, Av. du Président Pierre Angot, F-64000 Pau, France

<sup>3</sup>. CNRS, LCC (Laboratoire de Chimie de Coordination), 205 route de Narbonne, BP 44099, F-31077 Toulouse Cedex 4, France.

<sup>4</sup>. Université de Toulouse, UPS, INPT, F-31077 Toulouse Cedex 4, France

### **Experimental apparatus used for the synthesis.**

The experimental apparatus used in this work for the crystal synthesis, able to run experiments up to pressures of 200 bars and temperatures from -10 to 50 °C, is presented in Figure S11.

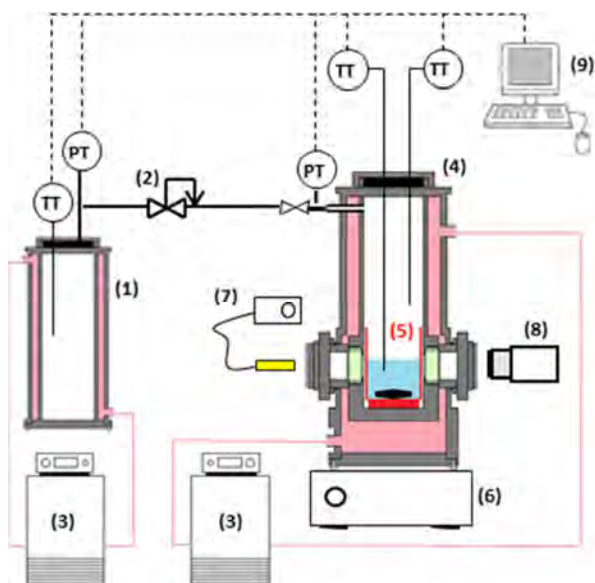


**Figure S11.** Scheme of the experimental rig. (1) gas storage vessel ; (2) pressure reducing valve; (3) thermostatic bath; (4) reactor; (5) glass vessel; (6) magnetic agitator; (7) optic fiber; (8) camera, (9) acquisition system.

The crystals of gas clathrate were synthesized in a jacketed high-pressure reactor of volume  $168.0 \pm 0.9 \text{ cm}^3$ , entirely made in 316L stainless steel. The reactor is equipped with two see through sapphire windows of 20 mm diameter arranged at  $180^\circ$  one from each other, which allows both lighting the interior of the reactor with an optical fiber (GBR150, Bodson) and recording the observations made using a commercial webcam (LiveCam Optia AF, Creative Labs). A small glass vessel, inserted in the reactor in such a way that the crystal formation can be monitored with the camera, contains the initial HQ solution. A star-shaped magnetic agitator driven by a magnetic stirrer (Hei-Mix D, Heidolph) is placed in the bottom of this glass vessel to reach the HQ-solvent solubility equilibrium at the beginning of the synthesis. The reactor temperature is regulated by means of a thermostatic bath (Polystat 37, Fisher Scientific), and two PT100 probes are located inside the reactor to measure the liquid and gas temperatures, with an accuracy of  $\pm 0.1^\circ\text{C}$ . The reactor is linked to a gas supply vessel maintained at constant temperature which contains the  $\text{CO}_2$  at sufficient pressure for the synthesis. The reactor pressure is adjusted using a pressure reducing valve (Dräger-Tescom) and measured with a 0-100 bar pressure transducer (Keller) with an accuracy of  $\pm 0.1$  bar. The whole system is monitored via a standard computer, and the data acquisition is done using a home-made LabView® interface with an acquisition frequency of 1 Hz.

To isolate the  $\beta$ -HQ crystals after the synthesis, four steps are necessary: (i) washing the crystals, (ii) separation of  $\alpha$ -HQ and  $\beta$ -HQ by density difference of the solids, (iii) filtration and (vi) drying. These steps are all performed in the same device – a jacketed glass Büchner funnel – to avoid any loss of solids during the successive operations. The low porosity of the filter used at the bottom of the Büchner allows maintaining a liquid or a suspension in the upper part of this apparatus when the vacuum filtration system is turned off. The temperature of the solution to be filtered is measured by an external temperature probe (model P650, Dostmann Electronic) with an accuracy of  $\pm 0.1$  K, and regulated by circulation of a propylene glycol solution in the Büchner jacket using a thermostatic bath. The solvent for these steps is  $\text{CH}_2\text{Cl}_2$ . The choice of  $\text{CH}_2\text{Cl}_2$  was triply motivated: (i) HQ is not soluble in  $\text{CH}_2\text{Cl}_2$ ; (ii) the range of density of this solvent with temperature is adapted for a separation of the  $\alpha$ -HQ and  $\beta$ -HQ crystals by floating; (iii) the low boiling temperature and high volatility of  $\text{CH}_2\text{Cl}_2$  facilitates the final drying step

#### **Characterization apparatuses and methods.**

Raman spectra were recorded on a T-64000 Jobin–Yvon spectrometer with a triple monochromator and 1800 grooves/mm gratings. The spectrometer was equipped with a confocal microscope. Spectra were recorded using the 514.5 nm line of an argon ion laser. The 200  $\mu\text{m}$  pinhole gave an 2  $\mu\text{m}$  axial resolution for surface analyses. The spectral field of view on the CCD detector was 400 nm to 1  $\mu\text{m}$ . The analysis was performed in the 3300 – 300  $\text{cm}^{-1}$  region with an acquisition time of 90 seconds under ambient conditions.

For infrared (IR) analysis, DRIFT spectra were collected on a Nexus Nicolet FTIR spectrometer flushed with dried air, with a resolution of 4  $\text{cm}^{-1}$  after signal averaging of 200 scans. The DRIFT spectra were recorded with the SPECTRA TECH Inc. collector diffuse reflectance accessory. A wideband, liquid-nitrogen-cooled mercury cadmium telluride (MCT) detector was used. HQ samples were diluted at 10% in a KBr matrix, previously dried at 373 K, and the mixture was ground before analysis. All the spectra were recorded against that of a pure KBr reference.

For the CPMAS  $^{13}\text{C}$  NMR experiments, a Bruker Avance 400 spectrometer operating at 100.61 MHz on the  $^{13}\text{C}$  and  $^1\text{H}$  resonance frequency of 400.13 MHz was used. Standard 7 mm zirconium dioxide rotors with a vespel drive cap were used with the Bruker MAS VTN 400 SB probehead. For all the measurements, the magic angle spinning speed was 7 kHz. A contact time of 3.8 ms was used, while a pulse delay of 5 s was chosen. A total of 2048 data points were acquired for each experiment. All data were collected at ambient temperature. More than 6000 scans were needed to obtain acceptable S/N (signal/noise) ratios for these samples. The spectrometer was calibrated with glycine before and during the NMR spectra acquisition. Chemical shifts, given in parts per million (ppm), were referenced to tetramethylsilane (TMS) at 0 ppm with sample substitution referencing the carbonyl signal in external glycine ( $\delta=176$  ppm). A line broadening (LB) of 4 Hz was applied to transform all the free induction decays (FIDs).

Optical transmission micrographs were recorded by sprinkling a few crystals on a clean glass cover slip on a Ti-Eclipse inverted microscope (Nikon) equipped with a DS-5Mc camera (Nikon). Colour images were converted to black and white grey scale to avoid source colour temperature artifacts. Images shown here underwent only linear contrast enhancement to highlight specific features (Fiji).<sup>1</sup>

Thermogravimetric analysis (TGA) was performed with a TGA SETSYS 1750 CS Evol. Helium at flowrate of 20 ml/min was introduced into the instrument. Samples were loaded onto the thermo-balance and heated from ambient temperature to 300°C at a rate of 5°C/min until a constant weight was obtained. The mass of the sample was continuously monitored, and a simultaneous analysis of the gas done by mass spectroscopy (OmniStar™ GSD 301 02), to identify the compounds responsible for the weight loss.

XRD analysis was performed at low temperature using an oil-coated shock-cooled crystal on a Bruker-AXS APEX II diffractometer with MoKa radiation ( $\lambda = 0.71073 \text{ \AA}$ ). The structure was solved by direct methods<sup>2</sup> and all non-hydrogen atoms were refined anisotropically using the least-squares method on  $F^2$ .<sup>3</sup> In order to avoid phase transition problems we repeated the measurement at different temperatures. We started at 233 K, followed by a measurement at 173 K to end up with an experiment at 100 K. The synthesis gave rise to a uniform sample of needle like crystals. One of these needles was cut to a reasonable size of  $0.4 \times 0.2 \times 0.2 \text{ mm}^3$  to perform the XRD analysis.

**HQ-CO<sub>2</sub> at 100K:** C<sub>18.87</sub>H<sub>18</sub>O<sub>7.74</sub>, Mr = 368.52, trigonal, space group  $R\bar{3}$ ,  $a = b = 16.202(2)$  Å,  $c = 5.694(4)$  Å,  $V = 1294.6(2)$  Å<sup>3</sup>,  $Z = 3$ ,  $T = 100(2)$  K, 5734 reflections collected, 857 unique reflections ( $R_{\text{int}} = 0.0163$ ),  $R1 = 0.0355$ ,  $wR2 = 0.0981$  [ $I > 2\sigma(I)$ ],  $R1 = 0.0362$ ,  $wR2 = 0.0987$  (all data), residual electron density =  $0.431 \text{ e \AA}^{-3}$ .

## Materials

The materials used for this study are listed in Table SII.

Table SII. Materials used for this study.

| Product           | Purity (mole %) | Supplier       |
|-------------------|-----------------|----------------|
| Hydroquinone      | 99 %            | Acros Organics |
| Ethanol Absolut   | >99%            | Sigma Aldrich  |
| Dichloromethane   | 99,99 %         | Acros Organics |
| Potassium bromide | >99%            | Sigma Aldrich  |
| Glycine           | >99%            | Sigma Aldrich  |
| Tetramethylsilane | >99%            | Sigma Aldrich  |
| Helium            | > 99,999 %      | Air Liquide    |
| Carbon dioxide    | > 99,995 %      | Linde gas      |

## References

- (1) Schindelin, J.; Arganda-Carreras, I.; Frise, E.; Kaynig, V.; Longair, M.; Pietzsch, T.; Preibisch, S.; Rueden, C.; Saalfeld, S.; Schmid, B. et al. *Nat. methods* **2012**, *9*, 676-682.
- (2) Sheldrick, G. M. *Acta Crystallogr.* **1990**, *A46*, 467-473.
- (3) Sheldrick, G. M. *Acta Crystallogr.* **2008**, *A64*, 112-122.